IET Networks

IET The Institution of Engineering and Technology WILEY

ORIGINAL RESEARCH

Leveraging InGaN solar cells for visible light communication reception

Habib Ullah Manzoor[1,2] | Sanaullah Manzoor[3] | Muhammad Ali Jamshed[1] | Tareq Manzoor[4]

[1]James Watt School of Engineering, University of Glasgow, Glasgow, UK

[2]University of Engineering and Technology, Lahore-FSD Campus, Lahore, Pakistan

[3]University of the West Scotland, Paisley, UK

[4]COMSATS University Islamabad, Lahore Campus, Islamabad, Pakistan

Correspondence

Tareq Manzoor.
Email: tareqmanzoor@cuilahore.edu.pk

Abstract

Solar cells are increasingly being utilised for both energy harvesting and reception in free-space optical (FSO) communication networks. The authors focus on the implementation of a mid-band p-$In_{0.01}Ga_{0.99}$ N/p-$In_{0.5}Ga_{0.5}$ N/n-$In_{0.5}Ga_{0.5}$ N (PPN) solar cell, boasting an impressive 26.36% conversion efficiency (under 1.5AM conditions) as a receiver within an indoor FSO communication network. Employing a solar cell with dimensions of 1 mm in length and width, the FSO system underwent simulation using Optisystm software, while the solar cell's behaviour was simulated using SCAPS-1D. The received power from the solar cell was then compared to that of four commercially available avalanche photodiode (APD) receivers. Exploring incident wavelengths spanning 400–700 nm within the visible spectrum, across transmission distances of 5, 10, 15, and 20 m, the study presented current-voltage (IV) and power-voltage curves. Notably, the InGaN solar cell exhibited superior electrical power output compared to all commercial APDs. In conclusion, the findings underscore that augmenting received power has the potential to enhance FSO network quality and support extended transmission distances.

KEYWORDS

free-space optical communication, optical communication, passive optical networks

1 | INTRODUCTION

5 G technology is poised to revolutionise modern communication networks, boasting the potential to enhance capacity by a remarkable factor of 1000 [1, 2]. However, the expansion of radio frequency communication's capacity has been hindered by limited spectrum resources [3, 4]. In the near future, downlink data rates could soar to 20 Gb/s, while uplink rates could reach 10 Gb/s [5]. To address escalating demand, researchers are increasingly investigating light as a communication medium [6–9].

Free-space optical (FSO) communications, also known as optical wireless communication (OWC), employ light as a wireless communication channel. Recent advancements in communication networks necessitate substantial bandwidth and superior network quality. While radio-frequency networks

offer restricted speed, FSO communication networks provide expansive bandwidth without the confines of frequency regulations [10, 11]. Moreover, FSO communication offers several advantages over conventional systems, including impressive bandwidth (up to 2000 THz), narrow beamwidth, unrestricted spectrum use, cost-effective installation, and flexible development opportunities [12]. Originally used in military applications [13] and inter-satellite links [14], FSO systems have evolved, with companies introducing innovative equipment for FSO communication systems [15–18], opening up new avenues for communication technology.

Five distinct categories of OWC systems exist based on transmission distance:

(i) Ultra-short range, such as chip-to-chip communication [19].

(ii) Short-range applications, including wireless body area networks, wireless personal area networks, and underwater communication [20, 21].

(iii) Medium-range scenarios, encompassing indoor infrared and visible light communication (VLC) for wireless local area networks [22].

(iv) Long-range OWC, such as inter-building connections.

(v) Ultra-long-range setups, such as inter-satellite links and deep space links [23, 24].

Remarkably, an OWC network capable of delivering 100 Gbps was successfully established for indoor illuminations [25]. Optical communication networks also align with the growing trend towards energy-efficient communication systems [26, 27], presenting a greener alternative that requires minimal hardware resources, thus aligning with cost-effective and environmentally friendly agendas [28]. Notably, due to light's inability to penetrate walls, OWC systems offer heightened security [29].

In contemporary light communication systems, either lasers or LEDs transmit light [11], while positive-intrinsic-negative diodes or avalanche photodiodes (APDs) serve as receivers [30]. A notable breakthrough occurred in 2013 when Kim and Won proposed the use of solar cells as receivers in FSO communication systems, simultaneously harnessing solar energy to generate electricity [31]. Subsequent studies explored the integration of polycrystalline Si solar cells [32], GaAs solar cells [33], organic solar cells [34], and perovskite solar cells [35] for light reception and energy harvesting. Intriguingly, the potential of InGaN solar cells for FSO communication remains untapped.

Recent investigations have spotlighted third-generation solar cells like InGaN solar cells, driven by their potential for high conversion efficiency [36–40]. The InGaN alloy boasts versatile applications in photodetectors, electronic devices [41], and laser diodes [42]. A distinguishing feature of InGaN lies in its adjustable direct wide bandgap, spanning from 0.7 eV (InN) to 3.42 eV (GaN) [43]. With excellent thermal stability and mobility, InGaN has the potential to replace Si in high-frequency optoelectronic and electronic applications, even in demanding environments [44].

This paper delves into the utilisation of InGaN-based solar cells as receivers in FSO communication networks for indoor settings. Specifically, a single-channel 100 Gbps FSO channel is evaluated. The study compares the FSO communication system's performance using a mid-band p-$In_{0.01}Ga_{0.99}$ N/p-$In_{0.5}Ga_{0.5}$ N/n-$In_{0.5}Ga_{0.5}$ N solar cell as an optical receiver to that with a conventional optical receiver. Leveraging Optisystem software for FSO communication system creation and SCAPS-1D software for solar cell evaluation, the research explores incident light varying from 400 to 700 nm, assessing FSO communication system performance based on received electrical power.

2 | SIMULATION SETUP

A 100 Gbps single-channel employing on-off keying (OOK) modulation was simulated using Optisystem software based on the previous work [45]. Developed by Optiwave System Inc., Optisystem offers comprehensive capabilities for simulating various optical communication systems. The OOK FSO network under consideration comprises three main components: the transmitter, FSO channel, and receiver.

The downlink transmitter comprises a non-return-to-zero pulse generator with a 0.5-bit duty cycle, driven by a pseudo-random bit sequence generator to achieve a 100 Gbps data rate. This signal is modulated using a continuous wavelength (CW) laser through a Mach–Zehnder modulator. The CW laser operates at a power of −20 dBm, covering wavelengths (λ) ranging from 400 to 700 nm. The optical signal produced by the Mach–Zehnder modulator is propagated through the FSO channel, varying in transmission lengths of 5, 10, 15, and 20 m. The FSO channels exhibit an attenuation of 25 dB/km and a beam divergence of 2 mrad.

At the receiver end, an APD with a responsivity of 1 A/W and a dark current of 10 nA is employed. Additionally, a low-pass filter with a cutoff frequency of 0.75 times the bit rate is utilised to convert the optical signals into electrical signals, as depicted in Figure 1. To ensure the proper functioning of FSO communication, eye diagram visualisers are utilised to obtain eye diagrams for all FSO channels at the receiving end, as illustrated in Figure 2. This comprehensive simulation and analysis framework provide insights into the performance and efficacy of the considered OOK FSO network.
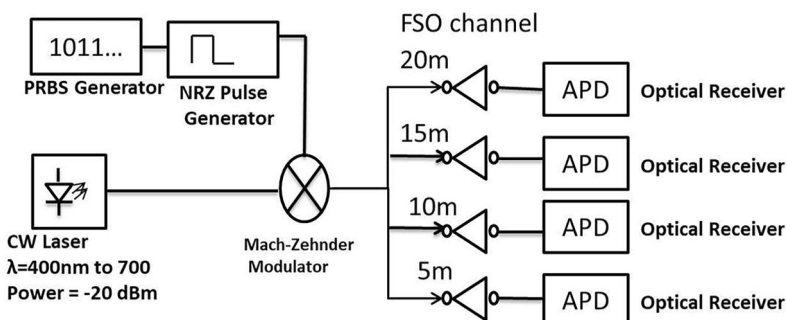

FIGURE 1 Schematic diagram of the single-channel on-off keying frees pace optical communication system.

3 | RESULTS OF FREE SPACE OPTICAL NETWORK

Figures 2a,b,c,d depict eye diagrams captured at transmission distances of 20, 15, 10, and 5 m, respectively, employing a wavelength (λ) of 700 nm. Notably, the clarity of the eye diagrams improves as the transmission distance decreases, with the 5 m distance exhibiting greater clarity due to diminished attenuation losses. The heights of the received eye diagrams correspond to 1.01×10^{-4} arbitrary units (a.u.) at 20 m, 1.37×10^{-4} a.u. at 15 m, 1.95×10^{-4} a.u. at 10 m, and 2.91×10^{-4} a.u. at 5 m. The received optical power was measured using an optical power meter at the FSO channel's end, while an electrical power meter gauged received electrical power at the receiver. Various commercially available APDs suitable for the visible light spectrum are detailed in Table 1.

These include APD15-8-150-T5H, APD230-LCC, MTAPD-06-001, and ADP120A2, produced by OSI Opto-electronics, Roithner Laser Technik, Marktech Optoelectronics,
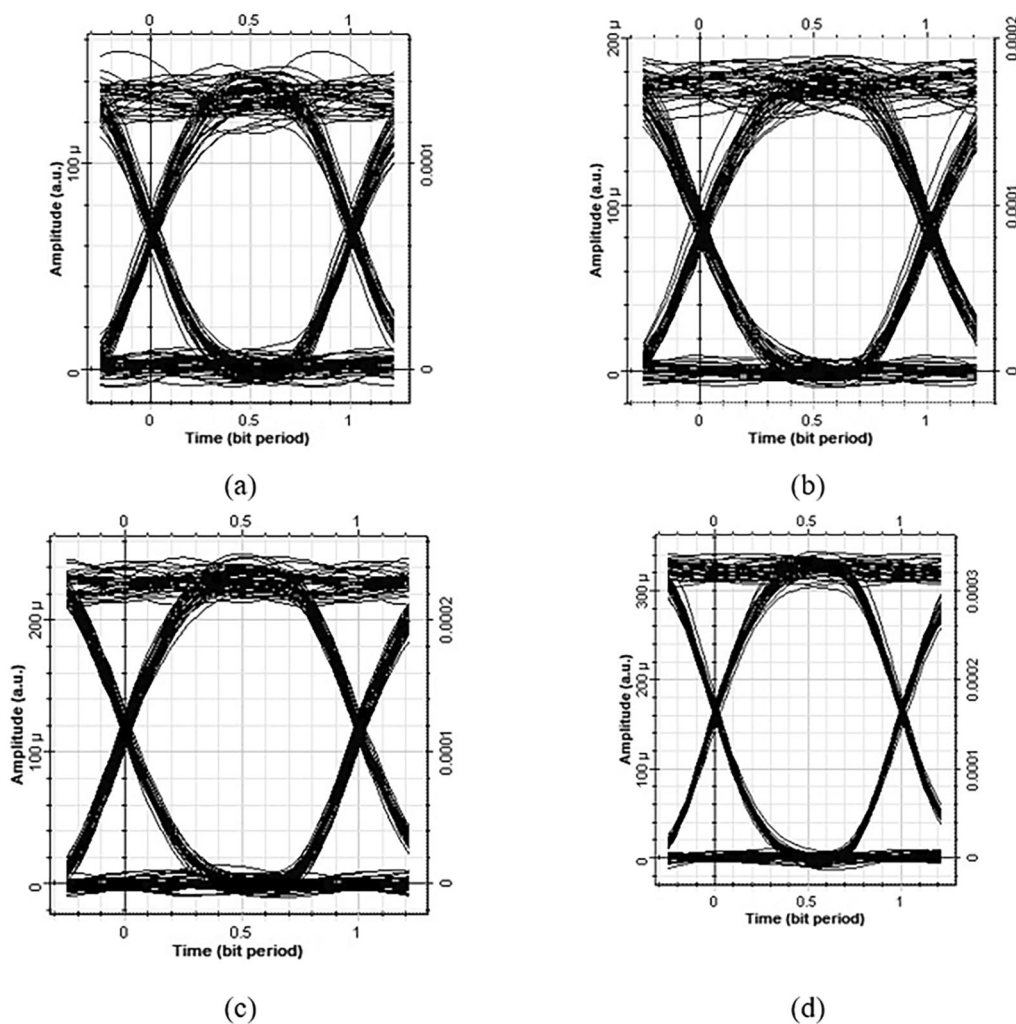

FIGURE 2 Eye diagram at the receiving end for a transmission distance of (a) 20 m, (b) 15 m, (c) 10 m, and (d) 5 m, at an incident wavelength of $\lambda = 700$ nm.

TABLE 1 Parameters of commercially available avalanche photodiodes.

ADP	Company name	Diameter (mm)	Wavelength (nm)	Dark current (nA)	Responsivity at (400–700 nm)(A/W)
APD15-8150-T5H	OSI optoelectronics	1.5	800	0.50	2–40
APD230LCC	Roithner laser technik	230.00	400–1100	0.20	0.5–27
MTAPD-06-001	Marktech optoelectronics	0.230	400–1100	0.05	5–40
ADP120A2	Thor labs	1	200–1000	-	12–25

Abbreviation: APD, avalanche photodiode.

TABLE 2 Received optical and electrical powers when ADP is used as the receiver.

Wavelength, λ (nm)	Transmission distance, (m)	Received optical power, (W)	Received electrical power, (W)			
			APD15-8-150-T5H	APD230LCC	MTAPD-06-001	ADP120A2
700	20	2.13E-05	1.35E-06	6.16E-07	1.35E-06	3.90E-07
	15	2.78E-05	2.25E-06	9.40E-06	2.29E-06	6.62E-07
	10	3.73E-05	4.13E-06	1.70E-05	4.14E-06	1.19E-06
	5	5.23E-05	8.13E-06	3.33E-05	8.13E-06	2.34E-06
600	20	2.13E-05	3.38E-07	3.38E-07	6.16E-07	5.07E-07
	15	2.78E-05	5.73E-07	5.15E-06	1.04E-06	8.60E-07
	10	3.73E-05	1.03E-06	9.32E-06	1.88E-06	1.55E-06
	5	5.23E-05	2.03E-06	1.83E-05	3.70E-06	3.05E-06
500	20	2.13E-05	2.11E-08	1.66E-07	6.84E-08	3.38E-07
	15	2.78E-05	3.58E-08	2.52E-06	1.16E-07	5.73E-07
	10	3.73E-05	6.48E-08	4.56E-06	2.10E-07	1.04E-06
	5	5.23E-05	1.27E-07	8.96E-06	4.12E-07	2.02E-06
400	20	2.13E-05	3.39E-09	2.28E-10	1.35E-08	1.22E-07
	15	2.78E-05	5.75E-09	3.25E-09	2.29E-08	2.06E-07
	10	3.73E-05	1.04E-08	5.85E-09	4.15E-08	3.73E-07
	5	5.23E-05	2.03E-08	1.15E-08	8.13E-08	3.72E-07

Abbreviation: APD, avalanche photodiode.

and Thor labs, respectively. Table 2 summarises the results of received optical and electrical powers. A notable trend in Table 2 indicates that APDs tend to perform more effectively with longer wavelengths, aligning with the influence of responsivity on optical receiver outputs [46]. Responsivity (R), a vital factor in APD performance, is approximately given by the equation [47]:

$$R \approx \frac{\eta\lambda}{1.24} \quad (1)$$

This Equation (1) underscores that responsivity increases proportionally with the applied wavelength of light.

4 | InGaN-BASED SOLAR CELL

In this study, the InGaN-based solar cell is composed of a three-layered PPN InGaN structure as depicted in Figure 3 [48]. The uppermost layer comprises p-In0.01GaN0.99 with a thickness of 0.1 μm, while the middle and bottom layers consist of p-In0.5GaN0.5 and n-In0.01GaN0.99 layers, each with a thickness of 1.0 μm. These layers possess a carrier density of 10^{19} cm^{-3}. The material parameters for all InGaN components utilised in the simulation are detailed in Table 3. The performance evaluation of this solar cell was conducted using the SCAPS-1D software, employing a 1.5 AM solar spectrum and operating at a temperature of 300 K.

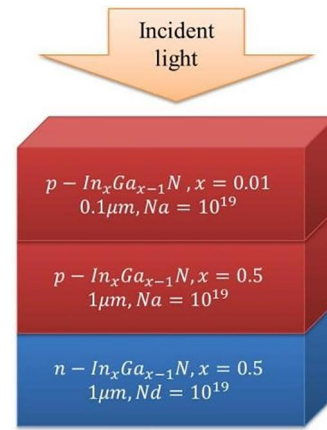Figure 4 illustrates the I-V and power-voltage (P-V) characterisics of the PPN InGaN solar cell. The simulation

FIGURE 3 An p-In$_{0.01}$Ga$_{0.99}$N/p-In$_{0.5}$Ga$_{0.5}$N/n-In$_{0.5}$Ga$_{0.5}$N (PPN) solar cell.

outcomes indicate that the cell can achieve an open circuit voltage (Voc) of 1.32 V, a current density (Jsc) of 21.95 mA/cm2, a fill factor of 90.37%, and a conversion efficiency (η) of 26.36%. Additionally, this cell demonstrates a power density of 26.4 mW/cm2.

4.1 | Solar cell as optical receiver

Figure 5 depicts the schematic diagram of a single-channel OOK FSO communication system utilising the

p-$In_{0.01}Ga_{0.99}$ N/p-$In_{0.5}Ga_{0.5}$ N/n-$In_{0.5}Ga_{0.5}$ N solar cell as the receiver. The solar cell, with dimensions of 1 mm × 1 mm, was subjected to a series of simulations using the SCAPS-1D

TABLE 3 Parameters for the InGaN solar cell.

| No.	Parameter	Value/Related equation
1	Bandgap, E_g [43]	$x. E_g^{InN} + (1 - x). E_g^{GaN} - b. x. (1 - x)$. Here $x = 0$–1, E_g^{InN} is 0.7 eV and E_g^{GaN} is 3.42 eV. The b is known as the bowing factor, which is equal to 1.43 eV.
2	Electron affinity, χ [49]	$4.1 + 0.7 (3.4 - E_g)$
3	Relative permittivity, ε [50]	$15.3x + 8.9 (1 - x)$.
4	Effective density state of the conduction band N_c [51]	$(0.9x + 2.3 [1 - x]) \times 10^{18}$ cm^{-3}
5	Effective density state of the valance band N_v [51]	$(5.3x + 1.8 [1 - x]) \times 10^{19}$ cm^{-3}
6	Carrier concentration	1×10^{19} cm^{-3}
7	Capture cross-section electrons	1.0×10^{-15} cm^2
8	Capture cross-section holes	1.0×10^{-15} cm^2
9	Defect density	1.0×10^{14} cm^{-3}
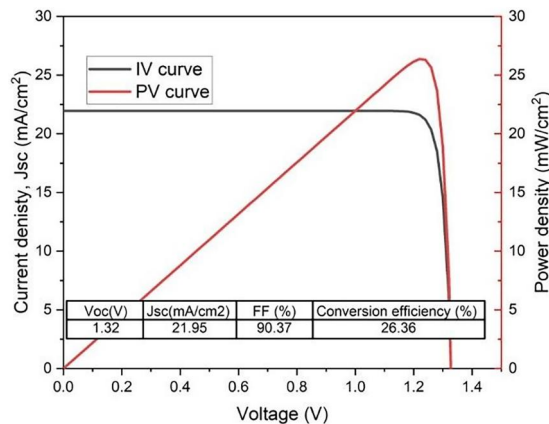
FIGURE 4 I-V and power-voltage curves of the PPN InGaN-based solar cell under 1.5 AM and temperature of 300 K.
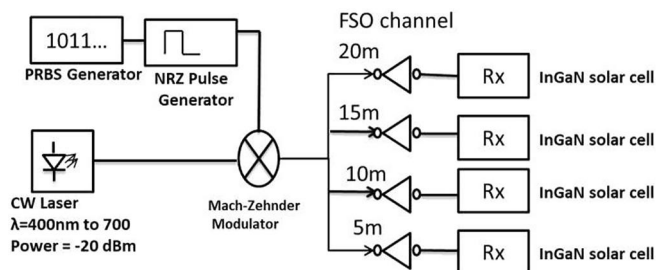

FIGURE 5 Schematic diagram of a single channel on-off keying frees pace optical communication system with the PPN InGaN solar cell as the receivers.

software. To emulate the optical received power from Optisystem software, as detailed in Table 2, the incident light's power was adjusted. These simulations were conducted across varying incident wavelengths within the visible spectrum, ranging from $\lambda = 400$ to 700 nm. The summarised results can be found in Table 4 and are graphically represented in Figure 6. Notably, the highest power generation occurred at $\lambda = 700$ nm, attributed to an increased responsivity at this wavelength. As λ decreases, the received electrical power proportionally decreases, although it remains superior to commercially available APDs. A comparison between Tables 2 and 4 suggests that the solar cell's

TABLE 4 Received optical and electrical power of a single channel on-off keying frees pace optical communication system with the PPN InGaN solar cell as the receivers.

| Wavelength, λ (nm)	Transmission distance, (m)	Received optical power, (W)	Received electrical power, (W)
700	20	2.13E-05	1.28E-05
	15	2.78E-05	1.66E-05
	10	3.73E-05	2.25E-05
	5	5.23E-05	3.20E-05
600	20	2.13E-05	1.15E-05
	15	2.78E-05	1.50E-05
	10	3.73E-05	2.02E-05
	5	5.23E-05	2.87E-05
500	20	2.13E-05	9.65E-06
	15	2.78E-05	1.25E-05
	10	3.73E-05	1.69E-05
	5	5.23E-05	2.39E-05
400	20	2.13E-05	8.67E-06
	15	2.78E-05	1.12E-05
	10	3.73E-05	1.52E-05
	5	5.23E-05	2.15E-05
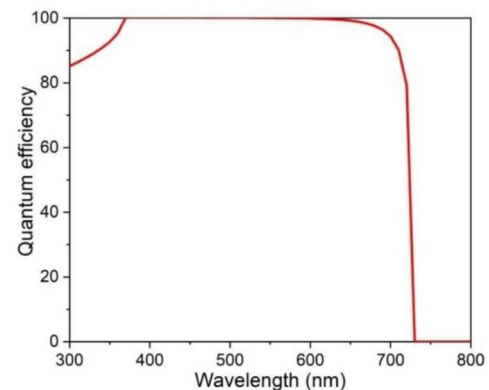
FIGURE 6 Specral Response of the p-$In_{0.01}Ga_{0.99}$ N/p-$In_{0.5}Ga_{0.5}$ N/ n-$In_{0.5}Ga_{0.5}$ N solar cell.

enhanced spectral response positions it favourably as a receiver for FSO communication networks, outperforming conventional APDs. The responsivity of the $p In_{0.01}Ga_{0.99}$ N/p-$In_{0.5}Ga_{0.5}$ N/n-$In_{0.5}Ga_{0.5}$ N solar cell can be evaluated using Equation (2) [52]:

Specral Response

$$= \frac{Quntaum\ Efficinecy \times\ Incident\ wavelength\ (nm)}{1239.8} \quad (2)$$

The Specral Response of the p-$In_{0.01}Ga_{0.99}$ N/p-$In_{0.5}Ga_{0.5}$ N/n-$In_{0.5}Ga_{0.5}$ N solar cell is depicted in Figure 6. Analysis indicates that the responsivity of this solar cell varies from 54 A/W to 34 A/W as the incident wavelength decreases from 700 to 400 nm. A comparison with Table 1 suggests that the p-$In_{0.01}Ga_{0.99}$ N/p-$In_{0.5}Ga_{0.5}$ N/n-$In_{0.5}Ga_{0.5}$ N solar cell delivers a more robust spectral response compared to APD15-8-150-T5H, APD230-LCC, MTAPD-06-001, and ADP120A2, consequently yielding higher output power. Spectral response data for APD15-8150-T5H, APD230-LCC, MTAPD-06-001, and ADP120A2 were obtained from their datasheets and are outlined in Table 1.

Figures 7a,b,c,d exhibit the I-V and P-V curves for different incident wavelengths and transmission lengths. A discernible reduction in the performance of the InGaN solar cell is evident as the incident wavelength declines from 700 to 400 nm. This behaviour aligns with the responsivity characteristics of the PPN InGaN solar cell. As presented in Figure 8, remarkably, an average optical power of 3.47E-05 W yields an average electrical power of 1.26E-06 W, 8.33E-07 W, 1.51E-06 W, and 9.75E-07 W for APD15-8-150-T5H, APD230LCC, MTAPD-06-001, and ADP120A2, respectively. In comparison, the InGaN solar cell produces 1.74E-05 W. Remarkably, the p-In0.01Ga0.99 N/p-In0.5Ga0.5 N/n-In0.5Ga0.5 N cell generates 13.9, 20.9, 16.1, and 17.9 times more power than APD15-8-150-T5H, APD230-LCC, MTAPD-06-001, and ADP120A2, respectively. Notably, all the commercially available APDs utilised in this study are silicon-based. The superior spectral response of PPN InGaN solar cells suggests their enhanced performance as VLC receivers.

Leveraging solar cells with energy-efficient devices can pave the way for self-powered networks [53], thereby reducing overall system costs by eliminating the need for batteries and minimising human intervention [54]. In such networks, the solar cell's energy can power devices like body-mounted sensors [55], pollution monitoring equipment [56], and medical devices [57]. With the discovery of new solar materials [58], solar cells will have more efficacy and will be able to perform better in these applications.
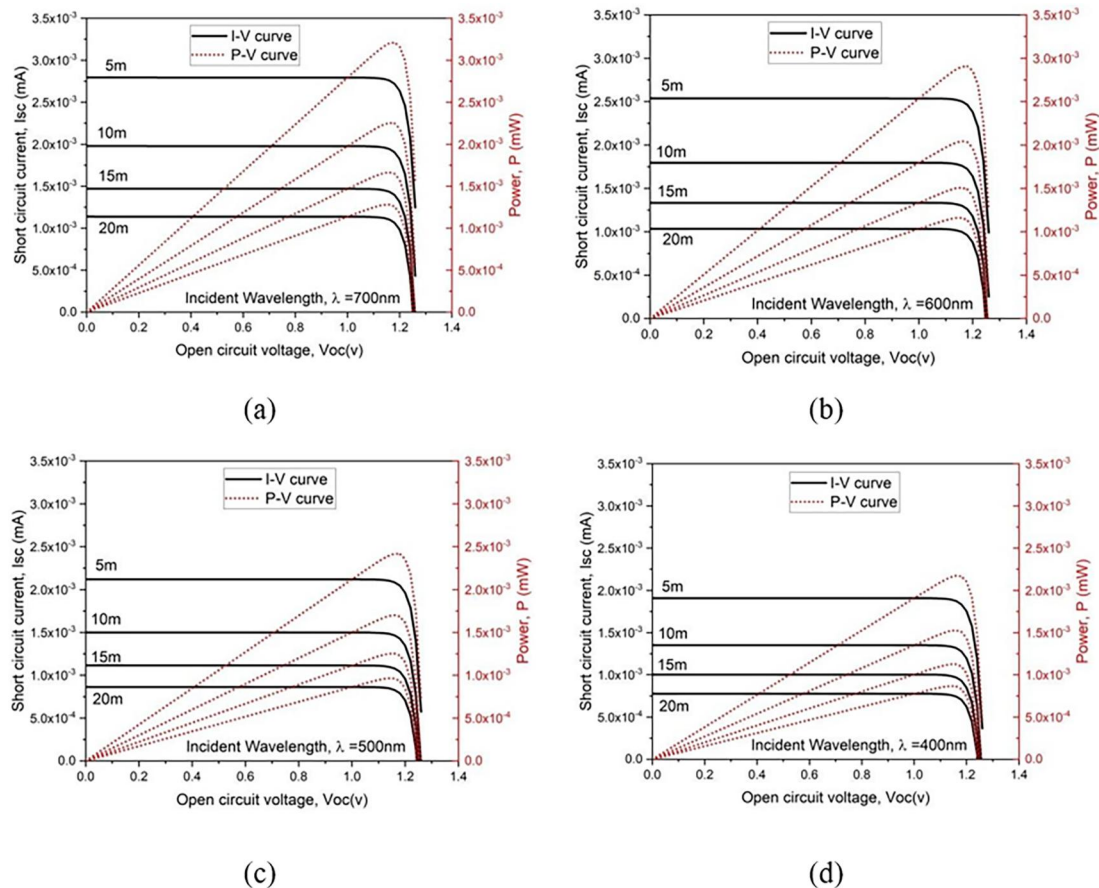

F I G U R E 7 I-V and power-voltage curves at different transmission lengths and different incident wavelengths: λ = (a) 700 nm, (b) 600 nm, (c) 500 nm, and (d) 400 nm.
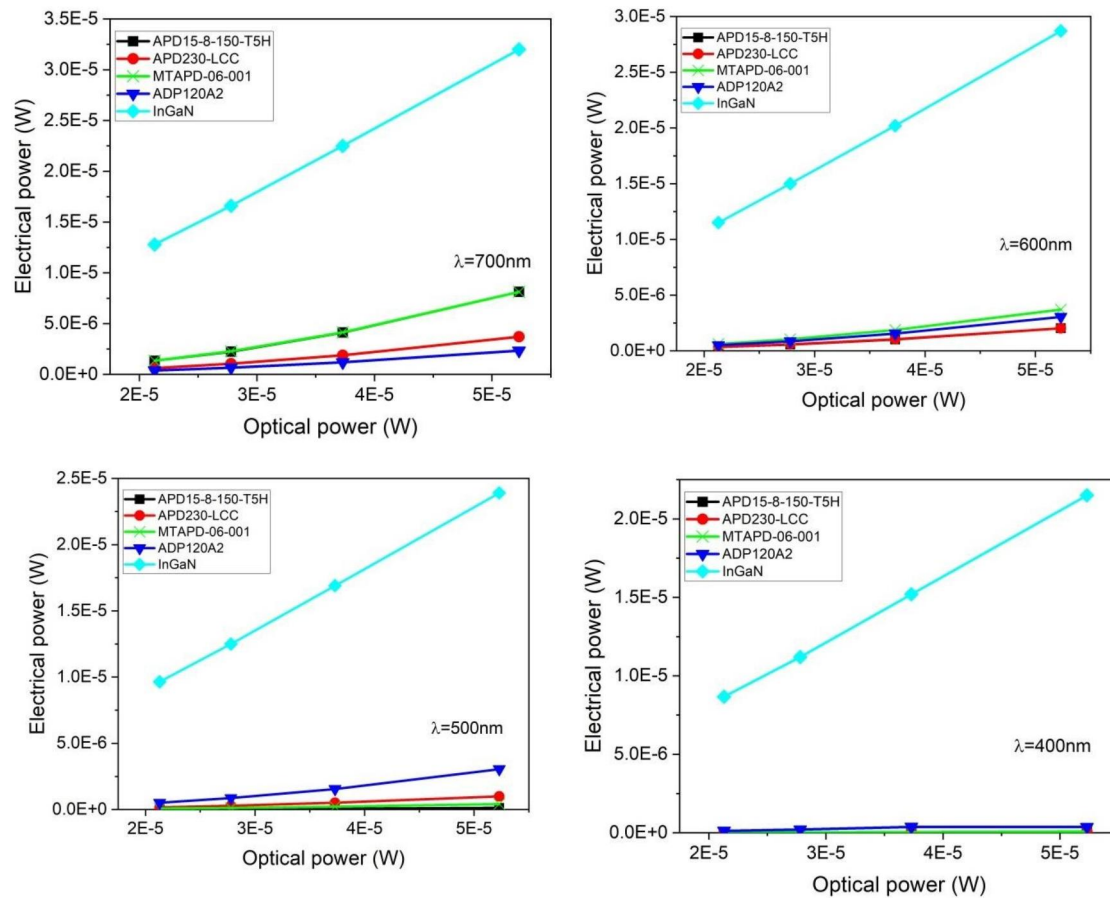
FIGURE 8 Received electrical power at the end of free-space optical channel at different incident wavelengths.

5 | CONCLUSIONS

Utilising solar cells as receivers in optical communication holds importance by enabling energy-efficient data reception, harnessing the power of ambient light to support sustainable and self-powered communication systems. This approach aligns with the growing emphasis on energy conservation and innovative integration of renewable resources within modern communication technologies. In this paper, we utilise a three-layered $p-In_{0.01}Ga_{0.99}$ N/$pIn_{0.5}Ga_{0.5}$ N/$n-In_{0.5}Ga_{0.5}$ N solar cell, boasting a remarkable 26.36% conversion efficiency under 1.5AM conditions, as an optical receiver in indoor FSO applications employing visible light. To evaluate its feasibility, we conducted simulations for a 100 Gbps downlink channel utilising the OOK modulation format within an FSO communication network. We employed four commercially available APDs alongside a PPN InGaN-based solar cell as the receiver. Remarkably, our $p-In_{0.01}Ga_{0.99}$ N/$p-In_{0.5}Ga_{0.5}$ N/$nIn_{0.5}Ga_{0.5}$ N solar cell exhibited superior output power compared to its commercial counterparts, including APD15-8-150-T5H, APD230-LCC, MTAPD-06-001, and ADP120A2. This heightened output power is poised to enhance the performance of the received signal, encompassing crucial metrics such as bit error rate, Q factor, and height of the eye diagram.

Furthermore, the amplified output power holds the potential to extend transmission distances, contributing to the overall robustness of the system.

AUTHOR CONTRIBUTIONS
Habib Ullah Manzoor: Conceptualisation; methodology; software; writing - original draft; resources; validation. **Sanaullah Manzoor**: Project administration; validation. **Muhammad Ali Jamshed**: Formal analysis; writing - review & editing; supervision. **Tareq Manzoor**: Review & editing.

CONFLICT OF INTEREST STATEMENT
The authors declare no conflicts of interest.

DATA AVAILABILITY STATEMENT
All data generated for this study is available through the mentioned software tools. Detailed instructions on reproducing the work, including the necessary steps and configurations, can be found in the manuscript. If further clarification or assistance is needed, please do not hesitate to contact the corresponding author.

ORCID
Habib Ullah Manzoor https://orcid.org/0000-0003-0192-7353
Sanaullah Manzoor https://orcid.org/0000-0002-4055-8469
Muhammad Ali Jamshed https://orcid.org/0000-0002-2141-9025

REFERENCES

1. Boccardi, F., et al.: Five disruptive technology directions for 5G. IEEE Commun. Mag. 52(2), 74–80 (2014). https://doi.org/10.1109/MCOM.2014.6736746

2. Larsson, E.G., et al.: Massive MIMO for next generation wireless systems. IEEE Commun. Mag. 52(2), 186–195 (2014). https://doi.org/10.1109/MCOM.2014.6736761

3. Salhab, A.M., et al.: Joint optimization of power allocation and load balancing for hybrid VLC/RF networks. J. Opt. Commun. Netw. 10(5), 553–562 (2018). https://doi.org/10.1364/JOCN.10.000553

4. Ghassemlooy, Z., et al.: Emerging optical wireless communications-advances and challenges. IEEE J. Sel. Area. Commun. 33(9), 1738–1749 (2015). https://doi.org/10.1109/JSAC.2015.2458511

5. Liu, X., Deng, N.: Emerging Optical Communication Technologies for 5G. Academic Press (2020). https://doi.org/10.1016/B978-0-12-816502-7.00019-1

6. Jeon, H.B., et al.: Free-space optical communications for 6G wireless networks: challenges, opportunities, and prototype validation. IEEE Commun. Mag. 61(4), 116–121 (2023). https://doi.org/10.1109/mcom.001.2200220

7. Lei, Q., et al.: Broadband transparent and flexible silver mesh for efficient electromagnetic interference shielding and high-quality free-space optical communication. Opt. Mater. Express 13(2), 469–483 (2023). https://doi.org/10.1364/ome.478830

8. Srinivasan, M., et al.: The Deep Space Optical Communications project ground laser receiver. In: Free-Space Laser Communications XXXV, vol. 12413, pp. 195–206. SPIE (2023)

9. Alhassan, A.M., et al.: Performance analysis of coherent source SAC OCDMA in free space optical communication systems. Symmetry 15(6), 1152 (2023). https://doi.org/10.3390/sym15061152

10. Aboelala, O., Lee, I.E., Chung, G.C.: A survey of hybrid free space optics (FSO) communication networks to achieve 5G connectivity for backhauling. Entropy 24(11), 1573 (2022). https://doi.org/10.3390/e24111573

11. Mohsan, S.A.H., Khan, M.A., Amjad, H.: Hybrid FSO/RF networks: a review of practical constraints, applications and challenges. Opt. Switch. Netw. 47, 100697 (2023). https://doi.org/10.1016/j.osn.2022.100697

12. Zhu, X., Kahn, J.M.: Free-space optical communication through atmospheric turbulence channels. EEE Trans. Commun. 50(8), 1293–1300 (2002). https://doi.org/10.1109/TCOMM.2002.800829

13. Rabinovich, W.S., et al.: Free space optical communications research at the U.S. Naval Research Laboratory. Proc. In: Free-Space Laser Communication Technologies XXII, vol. 7587, 758702. SPIE, San Francisco (2010). https://doi.org/10.1117/12.843682

14. Tolker-Nielsen, T, Oppenhauser, G.: In-orbit test result of an operational optical intersatellite link between ARTEMIS and SPOT4, SILEX. Proc. In: Free-Space Laser Communication Technologies XIV, vol. 4635, pp. 1–15. SPIE, San Jose (2002). https://doi.org/10.1117/12.464105

15. Killinger, D.: Free space optics for laser communication through the air. Opt. Photon. News 13(10), 36–42 (2002). https://doi.org/10.1364/OPN.13.10.000036

16. Komine, T., Nakagawa, M.: Fundamental analysis for visible-light communication system using LED lights. IEEE Trans. Consum. Electron. 50(1), 100–107 (2004). https://doi.org/10.1109/TCE.2004.1277847

17. Grubor, J., et al.: Broadband information broadcasting using LED-based interior lighting. J. Lightwave Technol. 26(24), 3883–3892 (2008). https://doi.org/10.1109/JLT.2008.928525

18. Li, Z., et al.: All silicon microdisplay fabricated utilizing 0.18 μm CMOS-IC with monolithic integration. IEEE Photon. J. 14(2), 1–5 (2022). https://doi.org/10.1109/jphot.2022.3160226

19. Feldman, M.R., et al.: Comparison between optical and electrical interconnections based on power and speed considerations. Appl. Opt. 27:105–108. (1987). https://doi.org/10.1364/ao.27.001742

20. IEEE standard for local and metropolitan area networks--Part 15.7: "Short-range wireless optical communication using visible light. IEEE Std 802157-2011, 1–309 (2011)

21. Hanson, F., Radic, S.: High bandwidth underwater optical communication. Appl. Opt. 47(2), 277–283 (2008). https://doi.org/10.1364/AO.47.000277

22. Gfeller, F., Bapst, U.: Wireless in-house data communication via diffuse infrared radiation. Inf. Syst. 5(3), 248 (1980). https://doi.org/10.1016/0306-4379(80)90043-5

23. Chan, V.W.S.: Optical satellite networks. J. Lightwave Technol. 21(11), 2811–2827 (2003). https://doi.org/10.1109/jlt.2003.819534

24. Hemmati, H. (ed.) Deep Space Optical Communications. Deep Sp. Opt. Commun, 11th ed. John Wiley & Sons (2006)

25. Tsonev, D., Haas, H., Videv, S.: Towards a 100 Gb/s visible light wireless access network. Opt Express 23(Issue 2), 1627–1637 (2015). https://doi.org/10.1364/OE.23.001627

26. Yang, Y., et al.: A novel hybrid dimming control scheme for visible light communications. IEEE Photon. J. 9(6), 1–12 (2017). https://doi.org/10.1109/JPHOT.2017.2771223

27. Chen, C., et al.: What is LiFi? J. Lightwave Technol. 34(6), 1533–1544 (2016). https://doi.org/10.1109/jlt.2015.2510021

28. Karunatilaka, D., et al.: LED based indoor visible light communications: state of the art. IEEE Commun. Surv. Tutorials 17(3), 1649–1678 (2015). https://doi.org/10.1109/COMST.2015.2417576

29. Zhang, Y.Y., et al.: Space codes for MIMO optical wireless communications: error performance criterion and code construction. IEEE Trans. Wireless Commun. 16(5), 3072–3085 (2017). https://doi.org/10.1109/TWC.2017.2675398

30. Kong, M., et al.: Survey of energyautonomous solar cell receivers for satellite–air–ground–ocean optical wireless communication. Prog. Quant. Electron. 74, 100300 (2020). https://doi.org/10.1016/j.pquantelec.2020.100300

31. Kim, S.-M., Won, Ji-S.: Simultaneous reception of visible light communication and optical energy using a solar cell receiver. 2013. Int. Conf. ICT Converg., 896–897 (2013). https://doi.org/10.1109/ICTC.2013.6675511

32. Wang, Z., et al.: On the design of a solar-panel receiver for optical wireless communications with simultaneous energy harvesting. IEEE J. Sel. Area. Commun. 33(8), 1612–1623 (2015). https://doi.org/10.1109/JSAC.2015.2391811

33. Fakidis, J., et al.: 0.5-Gb/s OFDM-based laser data and power transfer using a GaAs photovoltaic cell. IEEE Photonics Technol. Lett. 30(9), 841–844 (2018). https://doi.org/10.1109/LPT.2018.2815273

34. Zhang, S., et al.: Organic solar cells as high-speed data detectors for visible light communication. Opt 2 2(7), 607–610 (2015). https://doi.org/10.1364/OPTICA.2.000607

35. Natalie, A., et al.: Triple-Cation perovskite solar cells for visible light communications. Photon. Res. 8, A16–24 (2020). https://doi.org/10.1364/PRJ.393647

36. Zhao, Y., et al.: Toward high efficiency at high temperatures: recent progress and prospects on InGaN-based solar cells. Mater. Today Energy 31, 101229 (2023). https://doi.org/10.1016/j.mtener.2022.101229

37. Shan, H.S., et al.: High-efficiency InGaN photo cell irradiated by 532 nm laser with AlGaN electron blocking layer. ECS J. Solid State Sci. Technol. 12(7), 075007 (2023). https://doi.org/10.1149/2162-8777/ace73e

38. Sanmartín, P., et al.: Wide-bandgap III-V materials for high efficiency air and underwater optical photovoltaic power transmission. Sol. Energy Mater. Sol. Cell. 266, 112662 (2024). https://doi.org/10.1016/j.solmat.2023.112662

39. Shan, H.S., et al.: Enhancement of short-circuit current density in superlattice-based InGaN/GaN solar cells. ECS J. Solid State Sci.

Technol. 12(9), 095004 (2023). https://doi.org/10.1149/2162-8777/acfbb7

40. Chouchen, B., Khoja, I., Ladhari, T.: Artificial neural network modeling for optimization with high-efficiency in 0.2 Ga 0.8 N/GaN MQW solar cell at high temperature. In: 2023 IEEE International Conference on Artificial Intelligence & Green Energy (ICAIGE), pp. 1–5. IEEE (2023)

41. Yang, T., et al.: Green vertical-cavity surface-emitting lasers based on InGaN quantum dots and short cavity. Nano-Micro Lett. 15(1), 223 (2023). https://doi.org/10.1007/s40820-023-01189-0

42. Lu, Z., et al.: Recent progress of InGaN-Based red light emitting diodes. Micro and Nanostructures 183, 207669 (2023). https://doi.org/10.1016/j.micrna.2023.207669

43. Manzoor, H.U., et al.: Carrier density and thickness optimization of in. Sains Malays. 51(5), 1567–1576 (2022). https://doi.org/10.17576/jsm-2022-5105-24

44. Shan, H.S., et al.: Evaluation of photoconversion efficiency in InGaN/GaN MQW solar cells at high temperatures. ACS Appl. Energy Mater. 6(16), 8503–8510 (2023). https://doi.org/10.1021/acsaem.3c01351

45. Manzoor, H.U., et al.: Improved transmission length in the presences of ambient noise and scintillation effect using duobinary modulation in 40 Gbps free space optical channel. Microw. Opt. Technol. Lett. 62(10), 3163–3169 (2020). https://doi.org/10.1002/mop.32441

46. Agrawal, G.P.: Fiber-Optic Communication Systems, 4th ed Wiley (2012)

47. Jacobs, I.: Optical fiber communication technology and system overview. Conf. Proc. - IEEE S., 567–591 (1995). https://doi.org/10.1007/978-94-011-00359_29

48. Manzoor, H.U., et al.: High conversion and quantum efficiency indium-rich p-InGaN/p-InGaN/n-InGaN solar cell. Phys. B Condens. Matter 622, 413339 (2021). https://doi.org/10.1016/j.physb.2021.413339

49. Nawaz, M., Ahmad, A.: A TCAD-based modeling of GaN/InGaN/Si solar cells. Semicond. Sci. Technol. 27(3), 035019 (2012). https://doi.org/10.1088/0268-1242/27/3/035019

50. Zhang, X., et al.: Simulation of In0.65Ga0.35 N single-junction solar cell. J. Phys. D Appl. Phys. 40(23), 7335–7338 (2007). https://doi.org/10.1088/0022-3727/40/23/013

51. Tan, A.K., et al.: Numerical simulation of homojunction pin In0. 4Ga0. 6N solar cell with different absorber layer configurations. Optik 271, 170095 (2022). https://doi.org/10.1016/j.ijleo.2022.170095

52. Spectral Response | PVEducation n.d. https://www.pveducation.org/pvcdrom/solarcell-operation/spectral-response (Accessed 29 August 2021)

53. Dondi, D., et al.: Modeling and optimization of a solar energy harvester system for self-powered wireless sensor networks. IEEE Trans. Ind. Electron. 55(7), 2759–2766 (2008). https://doi.org/10.1109/TIE.2008.924449

54. Bi, S., Zeng, Y., Zhang, R.: Wireless powered communication networks: an overview. IEEE Wireless Commun. 23(2), 10–18 (2016). https://doi.org/10.1109/MWC.2016.7462480

55. Wu, F., Redoute, J.M., Yuce, M.R.: WE-safe: a self-powered wearable IoT sensor network for safety applications based on lora. IEEE Access 6, 40846–40853 (2018). https://doi.org/10.1109/ACCESS.2018.2859383

56. Wu, F., Rüdiger, C., Yuce, M.R.: Real-time performance of a self-powered environmental IoT sensor network system. Sensors 17(2), 282 (2017). https://doi.org/10.3390/S17020282

57. Hande, A., et al.: Self-powered wireless sensor networks for remote patient monitoring in hospitals. Sensors 6(9), 1102–1117 (2006). https://doi.org/10.3390/S6091102

58. Bhatti, S., et al.: Revolutionizing low-cost solar cells with machine learning: a systematic review of optimization techniques. Adv. Energy Sustain. Res. 4(10), 2300004 (2023). https://doi.org/10.1002/aesr.202300004